Fluidized Bed Synthesis of Carbon Nanotubes: Reaction Mechanism, Rate Controlling Step and Overall Rate of Reaction

Kinshuk Dasgupta
Rare Earths Development Section, Materials Group, Bhabha Atomic Research Centre, Trombay, Mumbai 400085, India

Dept. of Chemical Engineering, Institute of Chemical Technology, Matunga, Mumbai 400019, India

Jyeshtharaj B. Joshi
Dept. of Chemical Engineering, Institute of Chemical Technology, Matunga, Mumbai 400019, India

Homi Bhabha National Institute, Anushaktinagar, Mumbai 400094, India

Harvinderpal Singh
Rare Earths Development Section, Materials Group, Bhabha Atomic Research Centre, Trombay, Mumbai 400085, India

Srikumar Banerjee
Homi Bhabha National Institute, Anushaktinagar, Mumbai 400094, India

Bhabha Atomic Research Centre, Trombay, Mumbai 400085, India

DOI 10.1002/aic.14482
Published online May 9, 2014 in Wiley Online Library (wileyonlinelibrary.com)

Carbon nanotubes have been synthesized from acetylene and methane in a fluidized bed by using ferrocene as the catalyst dispersed over carbon black support material. The agglomerate size of carbon black, loading of catalyst, total gas flow rate, partial pressure of reactant gas, temperature of synthesis, and time of synthesis have been varied to understand their effects on the yield of carbon nanotubes. A reaction mechanism consisting of eleven steps and the rate equations for these steps have been proposed. Formation of carbon molecules on the catalyst surface was found to be the rate controlling step in the temperature range of 700–807°C, with an activation energy 47 kJ mol^{-1}, while diffusion through pores in the carbon black was found to be the rate controlling step in the temperature range of 807–1000°C with an activation energy of 7.6 kJ mol^{-1}. A continuous deactivation of the catalyst, represented by an exponential decay, was observed. The products have been characterized by thermogravimetry, electron microscopy, and Raman spectroscopy. © 2014 American Institute of Chemical Engineers *AIChE J*, 60: 2882–2892, 2014
Keywords: carbon nanotubes, chemical vapor deposition, fluidization, reaction mechanism, nucleation and growth

Introduction

Carbon nanotube (CNT) has been one of the most actively explored materials in recent year(s) due to its unique properties and wide range of applications.[1–3] However, the large-scale production of CNTs in an economic way is crucial for realizing these applications. Out of different techniques, catalytic chemical vapor depositions in fluidized bed[4–7] and in inclined mobile bed[8–11] reactors are the most promising techniques for the bulk production of CNT.

For designing of reactors, using basic principles, it is desirable to understand the mechanism, rate controlling steps and kinetics of the CNT synthesis. In this direction, substantial efforts are being made over a period of about past 10 years. Lee et al.[12] found that the rate is controlled by carbon diffusion inside the catalyst. Similar conclusion has been arrived by Helveg et al.,[13] Morancais et al.,[7] Philippe et al.,[5] Wirth et al.,[14] Anisimov et al.,[15] and Danafar et al.[16] However, for confirming the internal diffusion mechanism, it is important to investigate the effect of catalyst/support particle size on the kinetics of the process, an aspect which has not been covered in detail in the earlier studies. In view of this, Pirard et al.[17] reanalyzed the experimental data of Lee et al.,[12] and have shown that the rate is controlled by the surface reaction. Similar conclusion has been arrived by Pirard and coworkers[8–10] and Liu et al.[18] Thus, it can be seen that the published literature can be divided into two groups on the basis of controlling mechanism; one group proposing the reaction to be controlled by carbon diffusion

Correspondence concerning this article should be addressed to J. B. Joshi at jbjoshi@gmail.com, jb.joshi@ictmumbai.edu.in.

through the catalyst while according to the other group, the rate controlling step being the surface reaction.

From the foregoing discussion, it is clear that, additional work is needed for establishing the rate controlling step/s and kinetics. In particular, for gaining an understanding of the effects of catalyst particle size, the support size and the catalyst loading, it was felt desirable to undertake a systematic study over a wide range of most of these parameters.

There have been two additional motivations for undertaking the present work along with understanding the reaction mechanism. First, the choice of low cost support materials and reduction in downstream processing steps are the key factors for economic production of CNTs. To meet these requirements, we have chosen carbon black (N 330 grade, furnace black) as the support material. The attractive feature of carbon black is its primary particles of around 35-nm size which form soft agglomerate. Further, it can be obtained in various size ranges and can be easily fluidized without any preprocessing. On the contrary, mesoporous alumina, magnesia, and silica as catalyst-support materials[4,5,7] for CNT growth, require several steps of processing prior to fluidization. Similarly, ferrocene on cracking in inert atmosphere, deposits nascent iron (Fe) nanoparticle on the carbon black surface and it acts as the catalyst for CNT growth.[19] The separation of CNTs from carbon black can easily be achieved by preferential oxidation of the latter. Carbon black being disordered in nature gets oxidized earlier to CNTs. By using these low cost precursor materials in a fluidized bed furnace, we have been able to produce CNTs at the rate of 675 kg m^{-3} h^{-1}.

The third motivation for the current work is based on the observation that, in all the previous investigations,[8–11] the catalyst undergoes fast deactivation. Therefore, it was also thought desirable to seek the possibility of keeping the catalyst active for a longer duration during the course of the reaction.

Pirard et al.[20] have pointed out the importance of isothermal conditions in the reactor for avoiding the formation of soot and tars and for getting high productivity. In particular, isothermal conditions are useful for the elucidation of kinetics. Therefore, using fluidized bed method, four groups of researchers have performed systematic studies for the bulk production of CNTs. Serp and coworkers[5–7,21–24] have studied the effects of different parameters on CNT growth and have proposed a kinetic model of apparent chemical reactions. They observed the evolution of agglomerate structure during synthesis and proposed a growth model of CNT in a fluidized bed. Wei and coworkers[4,25–27] have reported a production rate of 5 kg per batch, however, discussed mainly macroscopic mechanism of CNT growth. They used a multiscale space-time analysis for scaled up production of CNT. Danafar and coworkers[16,28] have reported the influence of particle size and temperature on CNT growth. Harris and coworkers[29,30] have used factorial design to get the effects of different parameters. They observed a significant increase in pressure drop across the bed thus altering the hydrodynamics. All of four groups have given special focus on morphology and agglomeration behavior of the supported catalyst during fluidization. However, additional work has been felt necessary for establishing the rate controlling step/s and the kinetics.

Finally, it was considered worthwhile in revisiting the fluidized bed process and analyzing the data available in the published literature in view of the model developed in this work.

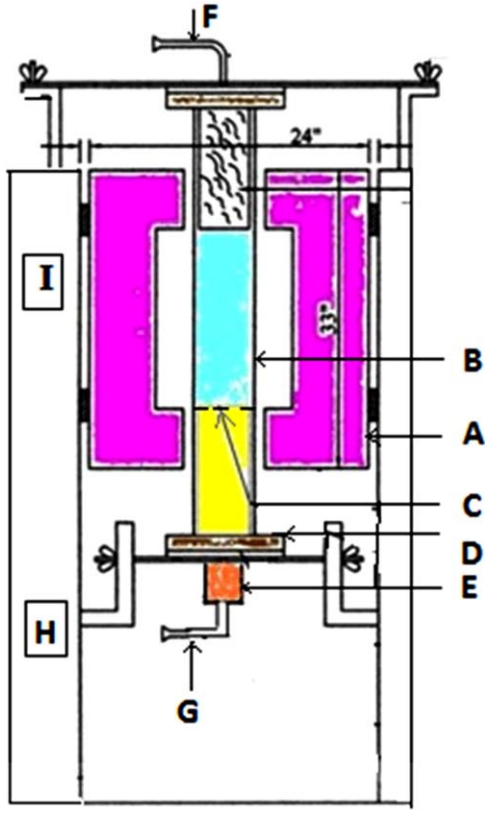

Figure 1. Experimental setup for production of CNT: (A) heater, (B) alumina tube, (C) Distributor, (D) water cooled flange, (E) preheater, (F) gas outlet, (G) gas inlet, (H) mass flow controller, and (I) temperature controller.

[Color figure can be viewed in the online issue, which is available at wileyonlinelibrary.com.]

Experimental

Experimental setup

The fluidized bed setup is shown in Figure 1. It is a vertical tubular furnace (A) having silicon carbide heating elements. An alumina tube (B) having inner diameter of 65 mm and length of 1000 mm. An alumina porous plate (C) of G3 porosity was employed as the distributor. There are water cooled top and bottom flanges (D), which support the alumina tube in a vertical position. A preheater (E) is attached below the bottom flange, where the desired quantity of catalyst is kept. The process gases enter through gas inlet (G) and go out from gas outlet (F). The gas flow is controlled by mass flow controllers (H). The temperature is measured by R type thermocouples and controlled by a proportional-integral-differential (PID) controller (I).

Materials and methods

Carbon black (N 330 grade) procured from HITECH Carbon Ltd. (Japan) was sieved into four different size ranges, namely, 90–150 μm, 150–210 μm, 210–250 μm, and 250–315 μm. Their fluidization behavior was observed by measuring the bed pressure drop against superficial gas velocity at room temperature and also at 700°C.

Carbon black was charged inside the furnace at room temperature and was initially fluidized by nitrogen till the temperature

of synthesis was reached. The entire process is divided into two steps, namely, catalyst deposition and CNT formation, which occur in series. Ferrocene, procured from M/s Aldrich, was charged inside the preheater, which was heated up to 250°C. At this temperature, ferrocene was vaporized and was carried into the furnace by nitrogen gas. Inside the furnace (kept at 700°C), ferrocene was cracked into Fe nanoparticles and deposited over the carbon black support material. The size of the Fe nanoparticles thus deposited ranges between 15 and 25 nm, which is reproducible. After 15 min, the temperature of the furnace was raised to the CNT synthesis temperature and acetylene/methane diluted with nitrogen (in desired ratio) was passed through the reaction bed where it cracked into C and H_2. The outlet gas stream composition was analyzed by gas chromatography using a capillary column. The CNT yield (in g) was measured by subtracting weight of the carbon black and catalyst from total weight of the carbon after each experiment.

To investigate the rate controlling step(s), experiments were performed in a systematic sequence. As we know, the CNT production rate could either be external mass transfer controlled or internal mass transfer (pore diffusion) controlled or reaction controlled. To understand the effect of external mass transfer, experiments were carried out over a wide range of gas superficial velocities ($5.03 \times 10^{-3} - 25.15 \times 10^{-3}$ ms^{-1} measured at standard condition). To understand the effect of pore diffusion, carbon black agglomerate size was varied within the range of 90–315 μm. These two sets of experiments were carried out over a wide range of temperatures (700–1000°C). The results at the highest temperature were used for elucidating the role of mass transfer. If the mass transfer is not important at the highest temperature, at a lower temperature the mass transfer steps remain increasingly unimportant because the activation energy for the mass transfer is always lower than that for the chemical reaction.

To understand the intrinsic kinetics, partial pressure of acetylene and methane (0.3–0.6 atm) and catalyst loading ($1 \times 10^{-3} - 20 \times 10^{-3}$ kg) were varied. The effect of temperature (700–1000°C) was studied to estimate the activation energy and the effect of time of synthesis (600–5400 s) was studied to understand the deactivation of catalyst.

It is worth mentioning here that the structure of the original carbon black got modified to fibrous structure during processing. The product contains CNT along with modified carbon black and catalyst particles. The product after each experiment was purified by treatment with dilute hydrochloric acid for 2 h, which removed most of the catalyst particles. Then, it was heated in air at 550°C for 1 h to remove the other forms of carbon except CNT. The temperature was decided based on thermogravimetric studies.[31] The analysis has been described in the characterization section. Differential scanning calorimetry (DSC) was also performed to get information regarding heat flow during oxidation.

The synthesized and purified products were characterized by Raman spectroscopy (ISI make), scanning electron microscope (SEM-model TESCAN VEGA MV23DDT/40) and transmission electron microscope (TEM-model JEOL 2000FX, 200 kV).

Results

Quality of fluidization

To get some idea about the quality of fluidization, the pressure drop across the bed (ΔP) was measured as a function of superficial gas velocity (V_G) at room temperature as well as at 700°C. The values of minimum fluidization velocities (V_{mf}) were found to be 2.95 and 2.75 mm s^{-1}, respectively. During the CNT formation experiments, the value of V_G was kept in the range of 5–10 times that of the minimum fluidization velocity. The pressure drop with respect to time was found to correspond with the actual weight of solid mass, which increased with time corresponding to the formation of CNT. These observations indicate that the fluidization was proper over the entire time of synthesis and also over the wide range of gas velocity used in the present work. During the process of CNT formation, the size and bulk density of carbon black particles increase. In a typical experiment, the average particle size increased from 120 to 130 μm and the bulk density increased from 300 to 375 kg m^{-3}. However, in all cases, the increase in the total weight was found to be equivalent to the formation of CNT.

Characterization of CNTs

Figure 2a shows thermogravimetry plots (weight loss with temperature) for the carbon deposit containing CNT produced at 800°C (solid line) along with that of original carbon black superimposed over it (dotted line). During heating in air, for individual sample, the weight loss starts at a particular temperature (points P and P′ in Figure 2a), which indicates the initiation of oxidation. The weight loss continues till all the carbon is burnt out (points Q and Q′ in Figure 2a). The catalyst remains as residue when carbon is burnt out. For the curve PQ (which corresponds to carbon black), there is no change in slope indicating a single rate of oxidation. Conversely, there is a change of slope for P′Q′ (which corresponds to the carbon deposit after the experiment), indicating two rates of reaction. The differential of plots PQ and P′Q′ are shown in Figures 2b and 2c, respectively. Figure 2b represents the rate of oxidation of the carbon black, where a single trough indicates a single oxidation reaction. Figure 2c represents the oxidation of carbon deposit containing modified carbon black and CNT. The first trough represents the oxidation of modified carbon black, which being disordered in nature starts oxidizing earlier. The second trough represents the oxidation of CNT. Figure 2d shows corresponding heat flow curves confirming the existence of two oxidation reactions. From the above figures, it is clear that the oxidation of carbon black starts by 450°C and gets over by 700°C. However, the oxidation of CNT starts after 670°C and continues till 870°C. Therefore, to separate out the CNTs, we first leached the product with dilute hydrochloric acid to remove the catalyst and then oxidized the product at 550°C for 1 h. This process ensured a significant removal of carbon black.

Figure 3a–d shows typical SEM images of CNT products at 700, 800, 900, and 1000°C after purification as described above. It can be observed that the diameter distribution is wider at 1000°C as compared to that at 700°C. Product at 800°C looks uniform. Figure 4a shows the TEM image of the CNT synthesized at 800°C. It is multiwall in nature with outer diameter 30–50 nm and the hollow core of CNT is visible. High resolution TEM image in Figure 4b reveals that the walls are well aligned. The distance between the walls is about 3.4 Å. The Raman spectrum of the initial product and that of the purified CNT showed characteristic "G" and "D" peaks. More the ratio of the intensity of the "G" peak to that of the "D" peak (I_G/I_D), greater is the ordering in the CNT wall. The purified CNT showed improved I_G/I_D. The above results show that the CNTs are of good quality.

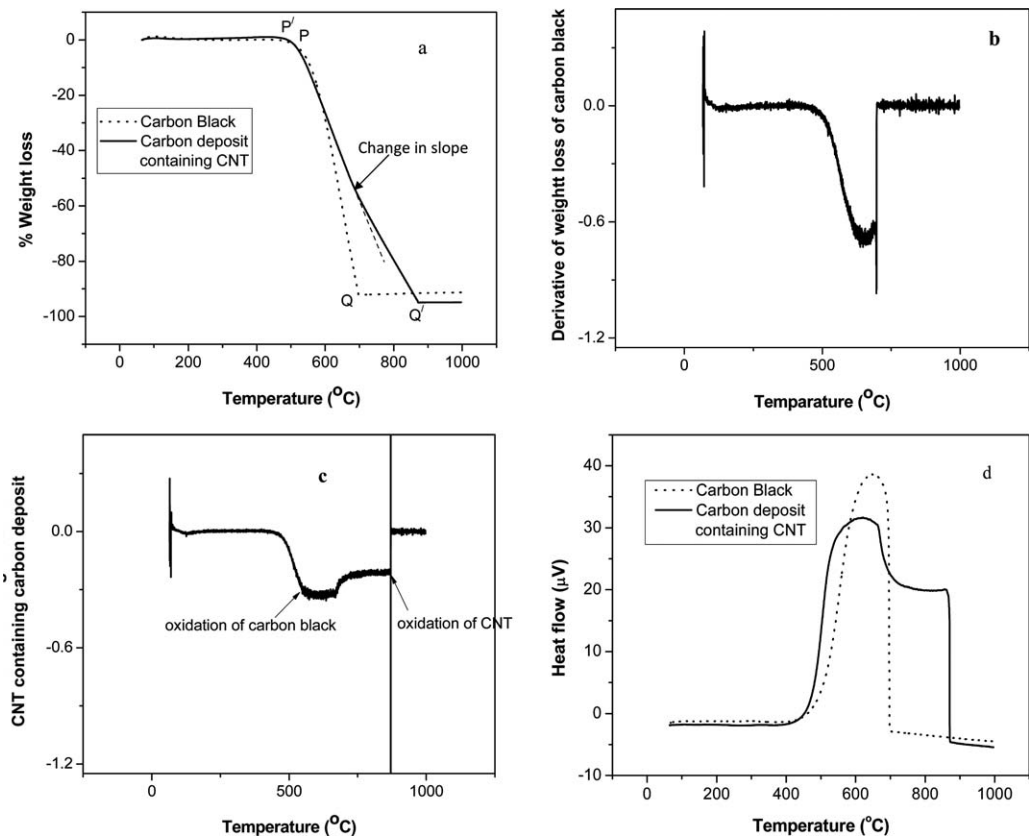

Figure 2. (a) Thermogravimetric plot for carbon black (CB) and carbon deposit containing CNT, (b) differential curve for the carbon black only, (c) differential curve for the carbon deposit containing CNT, and (d) DSC curve for the above two sample.

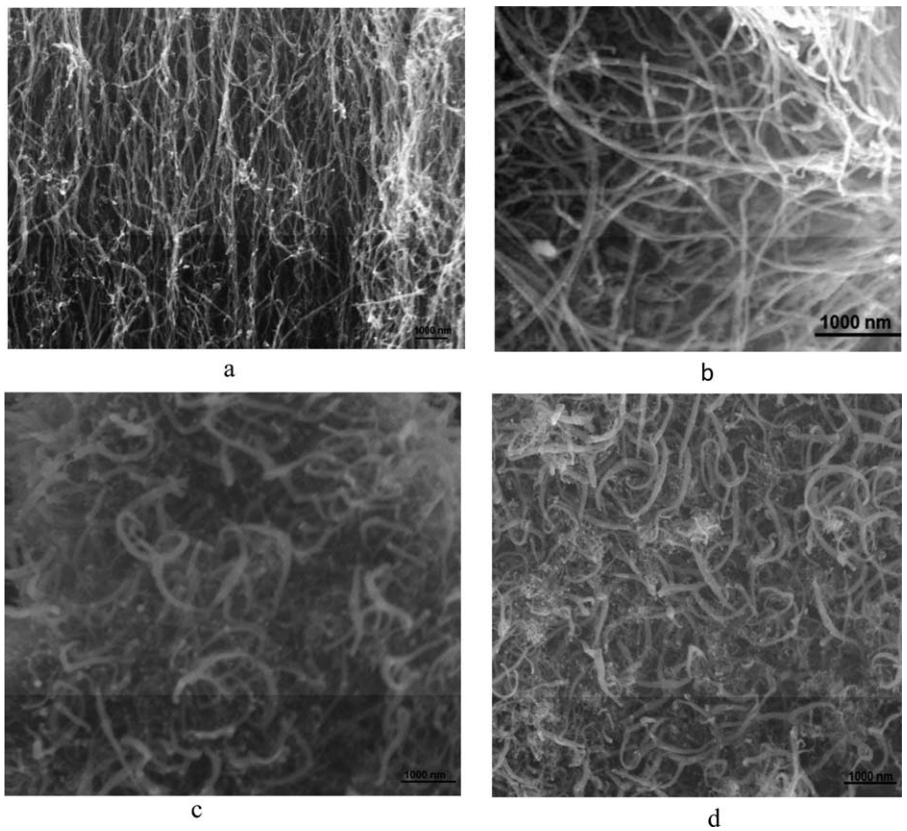

Figure 3. (a–d) SEM of the purified CNT product at 700, 800, 900, and 1000°C, respectively.

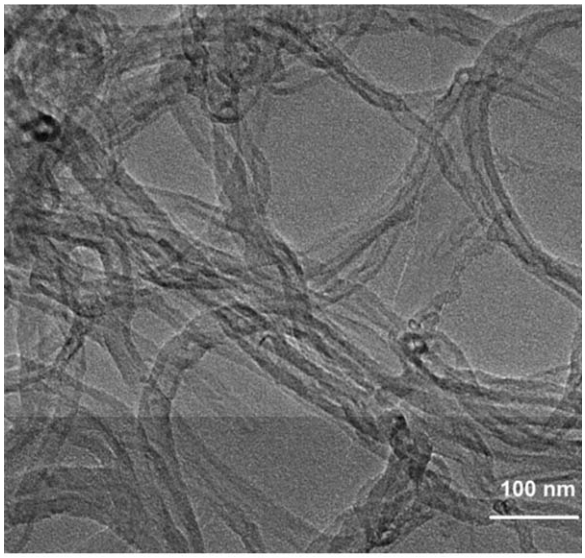

(a)

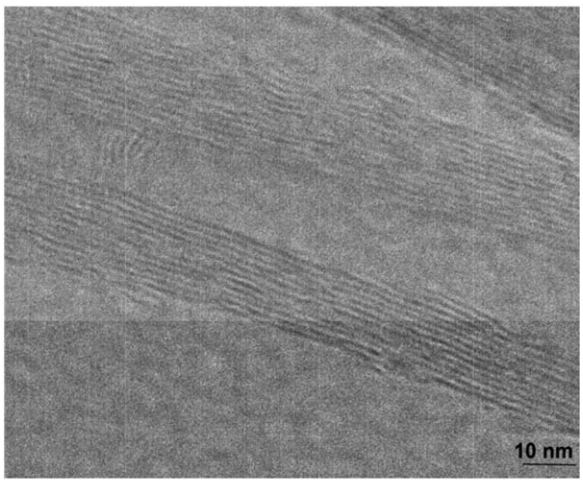

(b)

Figure 4. (a) TEM image of CNT produced at 800°C showing multiwall nature and (b) HRTEM image of CNT showing aligned walls of the tube.

Effect of total superficial gas velocity

The initial rate of formation of CNT, r^0_{CNT} (kg m^{-3} s^{-1}) has been used in this work, which can be defined as $r^0_{CNT} = \frac{1}{V}\left(\frac{dW_{CNT}}{dt}\right)_{t=0}$. A polynomial was fitted for W_{CNT} vs. time data and the value of r^0_{CNT} was obtained from the slope at $t = 0$ per unit volume (V) of reactor. Henceforth, r^0_{CNT} has been used where rate of CNT formation is concerned.

When the superficial gas velocity was increased from 5.03 $\times$ 10^{-3} to 25.15 $\times$ 10^{-3} ms^{-1} keeping partial pressure of acetylene and the carbon black agglomerate size constant, the CNT deposition rate did not vary significantly both at 800 and 1000°C (Table 1). This indicates that the external mass transfer may not be the rate controlling.

Table 1. Variation of CNT Deposition Rate with Gas Flow Rate Showing No Mass Transfer Resistance

Gas Flow Rate (ms^{-1})	CNT Deposition Rate at 800°C (kg m^{-3} s^{-1})	CNT Deposition Rate at 1000°C (kg m^{-3} s^{-1})
5.03 $\times$ 10^{-3}	0.08	0.094
10.06 $\times$ 10^{-3}	0.081	0.093
15.09 $\times$ 10^{-3}	0.081	0.093
25.15 $\times$ 10^{-3}	0.081	0.094

Effect of carbon black agglomerate size

Table 2 shows the effect of carbon black agglomerate size on the initial deposition rate of CNT at two different temperatures, namely, 800 and 1000°C with other parameters keeping constant. It can be seen that at 800°C, the agglomerate size does not have any significant effect on the CNT deposition rate whereas at 1000°C, it has. It means diffusion through pores of carbon black agglomerate has the effect on the CNT deposition rate at 1000°C. For spherical agglomerates, CNT deposition rate can be written as[32]

$$r^0_{CNT} = \frac{6(k\mathsf{D})^{0.5}}{D} p_{C_2H_2}$$

A linear fit of r^0_{CNT} with $1/D$ (Table 2) to the above expression, passing through origin, supports the pore diffusion control model.

Effect of catalyst concentration

Figure 5 shows the experimentally obtained CNT deposition rate at various C_t, at two different $p_{C_2H_2}$ at 800°C. It can be observed that the deposition rate varies linearly with catalyst concentration up to a point, after that saturation occurs. The saturation point depends on the total carbon input as acetylene. With higher $p_{C_2H_2}$, the deposition rate is higher for the same C_t. Thus, it can be seen that at partial pressures of 0.3 and 0.5 atm the CNT deposition rate reaches the saturation value at catalyst concentrations of 53 and 27 kg m^{-3}, respectively. In both the cases, total C input through acetylene was found to be the same (0.032 kg). Apart from contributing to the rate, the catalyst size determines the diameter of the CNTs. More about the role of catalyst is explained in the "Discussion" section.

Effect of partial pressure of acetylene

We have plotted the initial reaction rate, r^0_{CNT} with initial partial pressure of acetylene, $p^0_{C_2H_2}(T = 800°C)$, which is shown in Figure 6. Initially, we ensured that the extent of

Table 2. Dependence of CNT Deposition Rate with Carbon Black Agglomerate Size

Agglomerate Size (μm)	Bulk Density (kg m^{-3})	u_{mf} (mm s^{-1})	Bed Volume (m^3)	CNT Deposition Rate at 800°C (kg m^{-3} s^{-1})	CNT Deposition Rate at 1000°C (kg m^{-3} s^{-1})
90–150	340	2.95	1.47E-4	0.082	0.188
150–210	359	5.89	1.39E-4	0.081	0.135
210–250	356	11.79	1.4E-4	0.081	0.093
250–315	359	29.5	1.39E-4	0.082	0.086

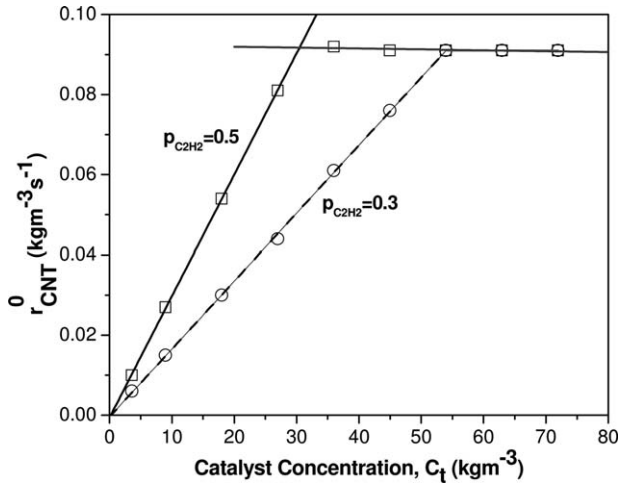

Figure 5. Effect of catalyst concentration on CNT deposition rate at different $p_{C_2H_2}$ showing linear dependence passing through origin before saturation concentration.

□ symbols denote deposition rates at $p_{C_2H_2} = 0.5$ atm and ○ symbols denote deposition rates at $p_{C_2H_2} = 0.3$ atm.

conversion is low (~30%) by keeping low concentration of catalyst ($C_t = 8.5$ kg m^{-3}). Further discussion pertaining to these results is given in the modeling section.

Effect of temperature

To get a preliminary feel of the effect of temperature, the initial deposition rate of CNT (ln r^0_{CNT}) was plotted vs. $1/T$ and is shown in Figure 7a. It can be observed that two different slopes exist over the entire temperature range (700–1000°C) indicating two different mechanisms are operating. At lower temperature range (700–807°C), the apparent activation energy is more, whereas at higher temperature range (807–1000°C) the apparent activation energy drastically reduces. The intrinsic activation energy will be calculated (later in this article) once the rate controlling steps are identified.

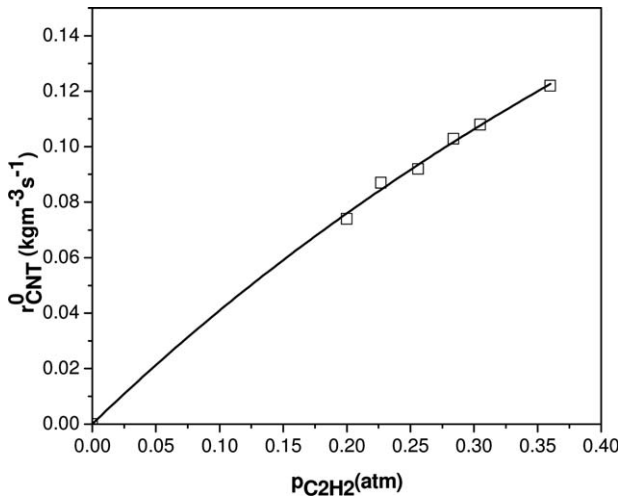

Figure 6. Variation of initial rate of CNT deposition rate withat 800°C.

The fit of mathematical model related to Step 5 suggests that formation of carbon molecule on catalyst surface is the rate controlling step.

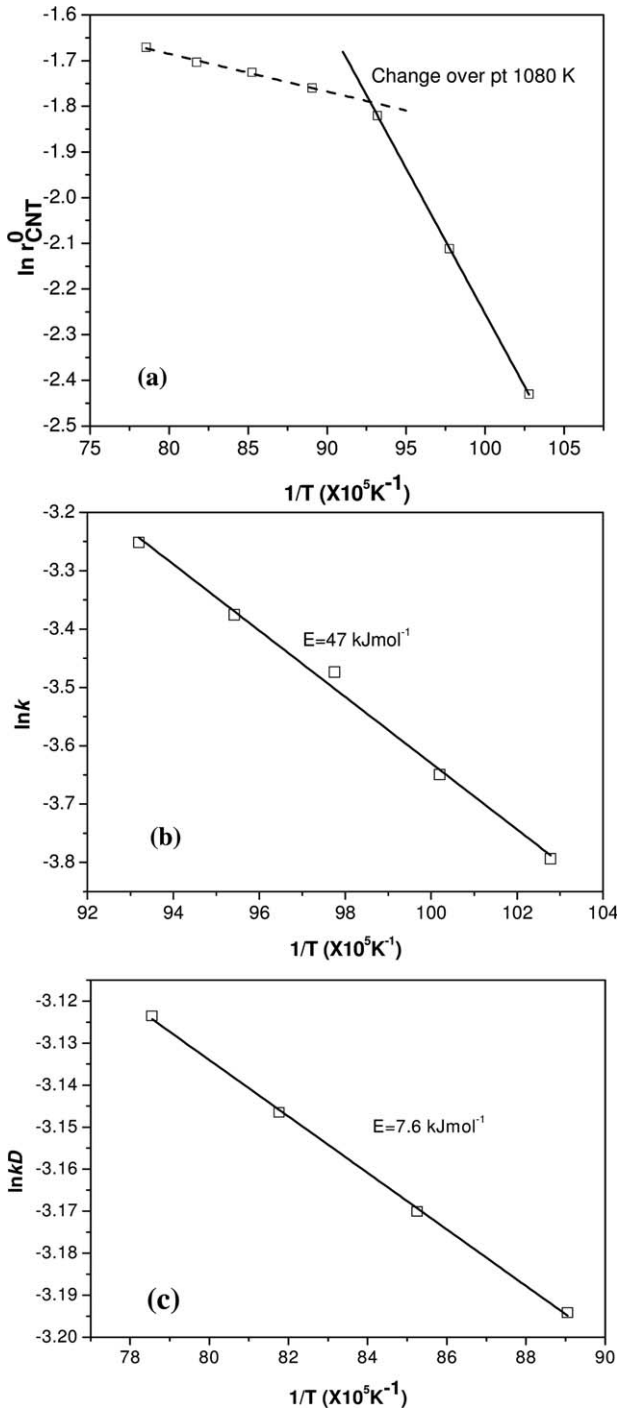

Figure 7. (a) Effect of temperature on initial reaction rate of CNT formation.

Existence of two slopes suggest two rate controlling steps in two different temperature regimes. (b) Plot to find intrinsic activation energy up to temperature 807°C. (c) Plot to find intrinsic activation energy in the temperature range of 807–1000°C

Discussion

Reaction mechanism

To understand the aforementioned observations, let us consider the various steps, which are involved in CNT synthesis in a fluidized bed (based on Kunii and Levenspiel[32]):

1. The hydrocarbon gas transfers from the bubble phase to the emulsion phase

2. Mass transfer of the hydrocarbon gas from emulsion to the external surface of the support (carbon black)
3. Diffusion of the hydrocarbon gas from the pore mouth on the surface to the surface of the catalyst
4. Adsorption of the hydrocarbon gas onto the catalyst surface (active site)
5. Reaction on the catalyst surface to produce carbon molecules
6. Dissolution of carbon molecules in the catalyst
7. Supersaturation of the catalyst with carbon
8. Nucleation and Growth of CNT
9. Desorption of hydrogen and other gaseous products
10. Diffusion of the gaseous products from the catalyst surface to the external surface of support (carbon black)
11. Mass transfer of gaseous products from support (carbon black) to the emulsion phase

Steps 1, 2, 3,10, and 11 are associated with low activation energies (<25 kJ mol^{-1}) and, therefore, cannot be the rate controlling step at lower temperatures (700–807°C) where the apparent activation energy is about 53 kJ mol^{-1} (initial estimation). Conversely, one or more of them may be the rate controlling in the higher temperature range (807–1000°C), where the activation energy is low (initial estimation 7 kJ mol^{-1}). To understand the effect of mass transfer, we analyzed the variation of CNT deposition rate with gas flow rate. Further, for understanding the effect of diffusion through pores, we analyzed the CNT deposition rate with carbon black agglomerate size.

From the results presented in Table 2, it may be concluded that the diffusion through pores (Step 3) is the rate controlling above 807°C as the rate of CNT formation is affected by the carbon black agglomerate size. Below 807°C any step among 4 to 8 may be the rate controlling, which can be represented by the following reactions with the rate constants given by k_i where i represents the step number

$$\text{Step 4: } C_2H_2 + S \underset{k_{-4}}{\overset{k_4}{\Longleftrightarrow}} C_2H_2.S$$

$$\text{Step 5: } C_2H_2.S \underset{k_{-5}}{\overset{k_5}{\Longleftrightarrow}} C_2.S + H_2$$

$$\text{Step 6: } C_2.S + C_2H_2 \underset{k_{-6}}{\overset{k_6}{\Longleftrightarrow}} [C]_S.S + H_2$$

$$\text{Step 7: } [C]_S.S + C_2H_2 \underset{k_{-7}}{\overset{k_7}{\Longleftrightarrow}} [C]_{SS}.S + H_2$$

$$\text{Step 8: } [C]_{SS}.S \overset{k_8}{\Rightarrow} [C]_S.S + CNT$$

Table 3. Predicted and Actual Weight of CNT at Different Catalyst Concentrations

Catalyst Conc (kg m^{-3})	Partial Pressure (atm)	Predicted CNT Weight (kg)	Actual CNT Weight (kg)
17.99	0.3	0.014	0.013
	0.35	0.016	0.015
	0.4	0.017	0.0164
	0.45	0.019	0.0185
	0.5	0.021	0.0194
	0.6	0.023	0.021
26.98	0.3	0.022	0.0197
	0.35	0.024	0.0227
	0.4	0.026	0.0244
	0.45	0.030	0.027
	0.5	0.032	0.029
	0.6	0.035	0.032

For any one of the above steps to be the rate controlling, the corresponding initial rates (r_i^0) are given by

$$\text{Step 4: } r_4{}^0 = k_4 p^0_{C_2H_2} C_t \quad (1)$$

$$\text{Step 5: } r_5{}^0 = \frac{K_4 k_5 p^0_{C_2H_2} C_t}{(1 + K_4 p^0_{C_2H_2})} \quad (2)$$

$$\text{Step 6: } r_6{}^0 = k_6 p^0_{C_2H_2} C_t \quad (3)$$

$$\text{Step 7: } r_7{}^0 = k_7 C_t \quad (4)$$

$$\text{Step 8: } r_8{}^0 = k_8 C_t \quad (5)$$

It can be observed that, all the rates given by Eqs. 1–5, vary linearly with catalyst concentration, C_t, and vary at different power levels with respect to $p_{C_2H_2}$ for all the cases. The observed linear dependence of the initial rate of CNT growth on catalyst concentration is shown in Figure 5. The initial reaction rate does not depend on initial partial pressure of acetylene if Step 7 or 8 is rate controlling. Conversely, it varies linearly with initial partial pressure of acetylene if Step 4 or Step 6 is rate controlling. For Step 5 to be rate controlling the relationship follows as per Eq. 2. The data points shown in Figure 6 suggest that Eqs. 1, 3–5 cannot be fitted well. The best fit is obtained with Eq. 2 (shown by solid black line). The values for k_5 and K_4 are as follow

$$k_5 = 0.0387 \pm 0.0025\ s^{-1}; \quad K_4 = 1.346 \pm 0.047\ Pa^{-1}$$

Further, to check the applicability of the rate equation for higher conversions, experiments were carried out with higher concentrations of catalyst. To find the extent of conversion at any time, Eq. 2 was integrated with the values of k_5 and K_4 given above. Table 3 shows excellent agreements between the predicted and the deposited CNT at higher catalytic concentrations (17.99 and 26.98 kg m^{-3} corresponding to 63.5% and 95% conversion). This suggests the validity of the rate equation for higher levels of conversion, too. Therefore, it can be concluded that in the lower temperature regime (<807°C), Step 5, that is, formation of carbon molecules on the catalyst surface is the rate controlling.

The intrinsic activation energies in the two temperature ranges, 700–807°C and 807–1000°C

Based on initial rates of reaction and reaction mechanism, the intrinsic activation energy has been determined. Figure 7b shows the plot of ln$k$ vs. 1/T in the temperature range of 700–807°C, where formation of carbon molecules on the catalyst surface is the rate controlling and the value of intrinsic activation energy is 47 kJ mol^{-1}. For pore diffusion control regime (807–1000°C) the plot of ln (kD) vs. 1/T yield the activation energy value of 7.6 kJ mol^{-1} (Figure7c).

Deactivation kinetics

The duration of synthesis was varied from 10 min (600 s) to 90 min (5400 s) both at 800°C and at 1000°C. A continuous decrease in CNT deposition rate can be seen at 800°C (Figure 8). It is due to the continuous deactivation of catalyst at 800°C, where the formation of carbon molecule on catalyst surface is rate the controlling. Out of different models available in the literature,[29] the following equation was chosen (based on best fit) to express the rate constant k_5

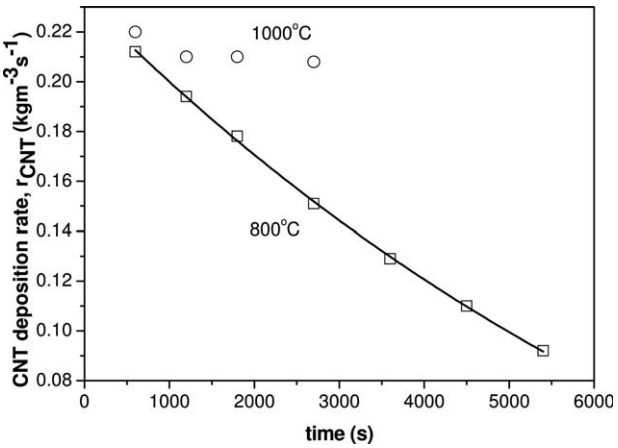

Figure 8. Plot of CNT deposition rate with time at two different temperatures.

□ symbols denote deposition rates at 800°C and ○ symbols denote deposition rates at 1000°C. There is continuous catalyst deactivation at 800°C, whereas at 1000°C there is no deactivation till 45 min (2700 s)

$$k_5 = A\exp(-\alpha t) + B \tag{6}$$

Equation 6 was fitted to the experimental points in Figure 8 which yield $A = 0.315\ s^{-1}$; $B = -0.082\ s^{-1}$; and $\alpha = 6.009 \times 10^{-5}\ s^{-1}$

At 1000°C temperature, practically no decrease in the CNT deposition rate could be observed till 45 min (2700 s) in contrast to the observation made at 800°C. The generation of carbon molecules on the catalyst surface has been identified to be the rate controlling step. Carbon molecules after getting dissolved into the catalyst come out as CNT when supersaturation occurs. Previous observations indicate that the deactivation is caused due to covering up of active catalyst surface by carbon, which is not forming CNT. At 800°C the rate of dissolution is less compared to that at 1000°C resulting in a faster deactivation at 800°C compared to that at 1000°C.

Effect of methane as precursor

To observe the effect of methane as precursor and also to validate the mathematical model given by Eq. 2, few experiments were carried out. The results are described below:

Effect of temperature: activation energy for methane. There was no change in slope in the entire temperature range (700–1000°C) for methane in contrast with that was in the case of acetylene. The activation energy for this case is found to be 47 kJ mol^{-1}in entire temperature ranges studied indicating diffusion through pore is not the rate controlling step. As methane is lighter hydrocarbon than acetylene, its diffusion is faster through pores. Moreover, acetylene is a polar compound and methane is nonpolar in nature. The polar acetylene interacts more with the surface groups present in carbon black. These together make the effective diffusivity of methane much more than acetylene in the pores of carbon black.

Validation of mathematical model. Figure 9 shows the CNT deposition rate at various inlet partial pressures of methane (p_{CH4}). The fit to Eq. 2 to the experimental data point suggest that formation of carbon molecules on catalyst surface is the rate controlling in this case also. The values for the rate constants are as follows:

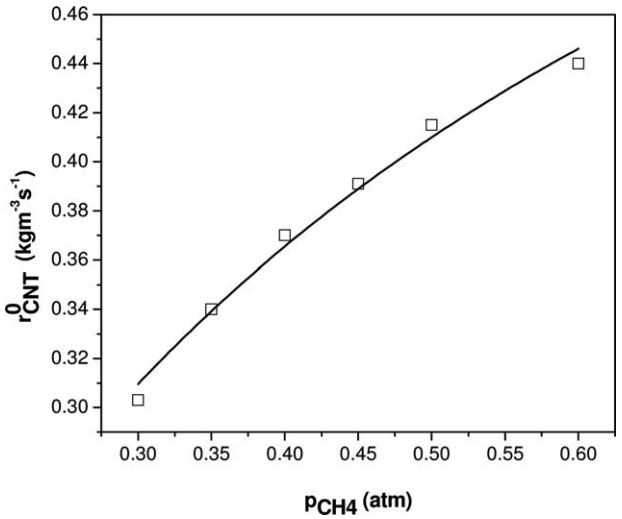

Figure 9. Variation of initial rate of CNT deposition rate with p_{CH4} at 800°C.

The fit of mathematical model related to Step 5 suggests that formation of carbon molecule on catalyst surface is the rate controlling step.

$$k_5 = 0.0625 \pm 0.0034\ s^{-1};\ K_4 = 33.82 \pm 1.95\ Pa^{-1}.$$

Analysis of published data in literature and comparison with the present work

For comparing our results with those published in the literature, we start with the fluidization behavior of the bed which is very important for scale up. Wang et al.[4] have used Fe impregnated alumina and magnesia powders. This group has given importance to control the agglomerate structure during synthesis of CNT in a fluidized bed. As per them, during synthesis, the size of the agglomerate increases but the density decreases resulting in rapid bed expansion. There exists a natural tendency to agglomeration due to van der Waals force amongst the supported catalyst and entanglement amongst CNTs synthesized. This can lead to defluidization of the bed unless proper care is taken with regard to catalyst design and operating parameters. Phillipe et al.[5,6] and Morancais et al.[7] has also used the Fe/Al_2O_3 catalyst and seen the tendency of agglomeration and defluidization with long duration of operation. They have also investigated kinetics which will be discussed later in this subsection. In present case, the agglomeration during operation has never been a problem as the CNTs were produced inside the porous structure of carbon black aggregate and the particle-size distribution remained within a narrow band which reduced the tendency of defluidization.

As per our calculation, the activation energy in the reaction controlled (formation of carbon molecules on the catalyst surface) regime is 47 kJ mol^{-1}. Similar value (59 kJ mol^{-1}) was reported by Snoeck et al.,[33] who proposed that reversible molecular adsorption of methane over Ni catalyst followed by abstraction of hydrogen atom was the rate controlling step. Hsieh et al.[34] found an activation energy of 26 kJ mol^{-1} over Fe/Al_2O_3 catalyst and 66 kJ mol^{-1} over Ni/Al_2O_3 catalyst during synthesis of MWCNTs from acetylene. Pirard et al.[35] reported a value of 130 kJ mol^{-1} during decomposition of ethylene over $Co\text{-}Fe/Al_2O_3$ system. In the pore diffusion control regime, we have found the activation energy of 7.6 kJ mol^{-1}. Using ethylene over Fe/Al_2O_3,

Table 4. Experimental Variables Used for CNT Synthesis by Four Authors, Whose Data have been Analyzed by Our Model

Ref.	Support	Catalyst	Carbon Source	Equipment	k_5	K_4
Douven et al.[10]	Magnesia	Fe/Co	Methane	Rotating bed	0.532	7.64
Pirard et al.[9]	Alumina	Fe/Co	Ethylene	Rotating bed	0.766	42.35
Philippe et al.[36]	Alumina	Fe	Ethylene	Fluidized bed	0.034	13.5
Gommes et al.[37]	Alumina	Fe/Co	Ethylene	Rotating bed	0.61	30.15
Our data	Carbon black	Fe	Acetylene	Fluidized bed	0.0387	1.346

Philippe et al.[6] found an activation energy of 29 kJ mol^{-1}, where diffusion through alumina particle was found to be the rate controlling.

There are few published articles where the authors have reported the CNT deposition rate with the initial partial pressure of the reactants. Table 4 summarizes the experimental conditions and the equipment used by them. Figure 10 presents these data and depicts the fit of the model to their data along with us developed in this work. From the plots, it is clear that the present model fits well to these data. The values of rate constants (k_5 and K_4) for them are tabulated in Table 4. It is to be noted that some reported data[7,16] follow the rate controlling step to be diffusion controlled. As per our analysis below 807°C, the rate of CNT formation is reaction controlled and above this temperature it is internal diffusion controlled. Therefore, it may be noted that the rate controlling step depends on regime of operation and the system concerned.

Summary and Conclusions

1. We have used a fluidized bed to produce CNT. Ferrocene has been used as the catalyst, dispersed on carbon black (N 330 grade) support material. Acetylene and methane have been used as the source of carbon and nitrogen is the carrier gas.
2. The mechanism of CNT formation in the fluidized bed comprises of eleven steps, namely, mass transfer of the hydrocarbon gas from bubble phase to emulsion phase, mass transfer of hydrocarbon from emulsion to the external surface of the support (carbon black), diffusion of hydrocarbon from the pore mouth of the carbon black to the active surface of the catalyst, adsorption of the hydrocarbon onto the catalyst surface (active site), reaction on the catalyst surface to produce carbon molecules, dissolution of carbon molecules in the catalyst, supersaturation of the catalyst with carbon, nucleation and growth of CNT, desorption of hydrogen and other gaseous products, diffusion of the gaseous products from the catalyst surface to the external surface of support (carbon black) and mass transfer of gaseous products from support (carbon black) to the emulsion phase.
3. To determine the rate controlling step, several experiments were carried out with varying temperature, superficial gas velocity, partial pressure of acetylene and methane, catalyst concentration, agglomerate size of carbon black, and synthesis duration.
4. Formation of carbon molecules on the surface of the catalyst was found to be the rate controlling in the temperature range of 700–807°C for acetylene as feed gas, where activation energy was 47 kJ mol^{-1}. At higher temperature range (807–1000°C), rate controlling mechanism shifted to diffusion through pores of carbon black, with activation energy 7.6 kJ mol^{-1}. There was a continuous deactivation of catalyst which we have represented by an exponential decay model. The values of the rate constants as well as the deactivation kinetics have been reported in this work.
5. To validate the rate controlling step, the published results on the CNT synthesis by four authors (Ref. 9,10,36,37) have been analyzed as per our model. It may be noted from Table 4, that these results cover different support materials, carbon sources, catalysts, and temperatures.
6. We have also used methane as a carbon source. Formation of carbon molecules on the surface of the catalyst was found to be the rate controlling in the entire temperature range of 700–1000°C with an activation energy of 47 kJ mol^{-1}. The lighter and nonpolar nature of methane makes its diffusion faster.
7. In this work, it has been shown that the productivity of 675 kg m^{-3} h^{-1} can be obtained.
8. This article brings out (a) the rate controlling step and (b) the estimation of the rate of CNT synthesis in a fluidized bed. These results are expected to be very useful for the purpose of scale-up.
9. The present work is concerned with the mechanism and kinetics of CNT synthesis. It is suggested that the future work includes the simulations using computational fluid dynamics[38] and its relationship with heat transfer[39]and mixing.[40,41] The turbulence structure[42,43] within the reactor need also be investigated for getting additional knowledge on transport phenomena.

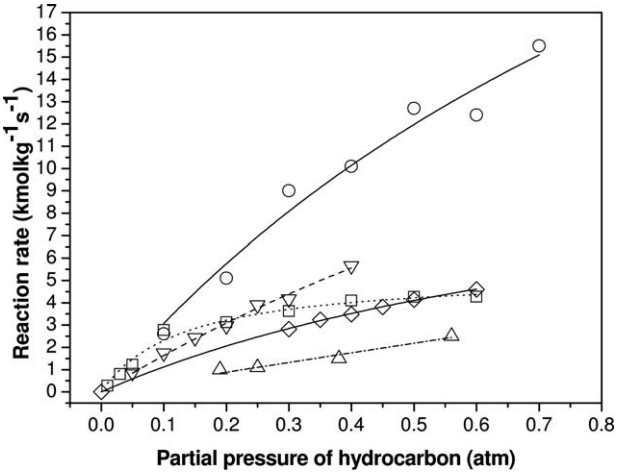

Figure 10. Analysis of reported data in literature by fitting our model.

○ Douven et al.,[10] □ Pirard et al.,[9] Δ Philippe et al.,[36] Gommes et al.,[37] our data.

Notation

α = deactivation constant, s^{-1}
A = pre-exponential constant in Eq. 6, s^{-1}

B = rate constant component in Eq. 6, s^{-1}
C_2 = carbon molecule
C_2H_2 = acetylene
$C_2H_2.S$ = acetylene adsorbed on catalyst active site
$C_2.S$ = carbon molecule adsorbed on catalyst active site
$[C]_S.S$ = catalyst saturated with carbon
$[C]_{SS}.S$ = catalyst supersaturated with carbon
C_t = concentration of total catalyst, kg m^{-3}
D = diameter of agglomerate, m
D = diffusivity, $m^2\ s^{-1}$
E = activation energy, J mol^{-1}
H_2 = hydrogen
k_4 = rate constant for forward reaction for Step 4, $Pa^{-1}\ s^{-1}$
k_{-4} = rate constant for backward reaction for Step 4, s^{-1}
k_5 = rate constant for forward reaction for Step 5, s^{-1}
k_{-5} = rate constant for backward reaction for Step 5, $Pa^{-1}\ s^{-1}$
k_6 = rate constant for forward reaction for Step 6, $Pa^{-1}\ s^{-1}$
k_{-6} = rate constant for backward reaction for Step 6, $Pa^{-1}\ s^{-1}$
k_7 = rate constant for forward reaction for Step 7, $Pa^{-1}\ s^{-1}$
k_{-7} = rate constant for backward reaction for Step 7, $Pa^{-1}\ s^{-1}$
k_8 = rate constant for forward reaction for Step 8, s^{-1}
$K_4 = k_4/k_{-4}$ equilibrium constant for Step 4, Pa^{-1}
$p_{C_2H_2}$ = partial pressure of acetylene, Pa
$p^0_{C_2H_2}$ = initial partial pressure of acetylene, Pa
ΔP = pressure drop across bed, Pa
r_{CNT} = deposition rate of CNT, kg $m^{-3}\ s^{-1}$
r^0_{CNT} = initial deposition rate of CNT, kg $m^{-3}\ s^{-1}$
R = universal gas constant, J $mol^{-1}\ K^{-1}$
S = active site on catalyst
t = time of deposition, s
T = temperature, K
V_{mf} = minimum fluidization velocity, mm s^{-1}
V = volume of the bed, m^3
V_G = superficial gas velocity, mm s^{-1}
W_{CNT} = weight of CNT, kg

Literature Cited

1. Baughman RH, Zakhidov AA, de Heer WA. Carbon nanotubes—the route toward applications. *Science*. 2002;297:781–787.
2. Dillon AC, Jones KM, Bekkedahl TA, Kiang CH, Bethune DS, Heben MJ. Storage of hydrogen in single-walled carbon nanotubes. *Nature*. 1997;386:377–379.
3. Fan JP, Zhang DM, Zhao DQ, Zhang G, Wu MS, Wei F, Fan ZJ. Toughening and reinforcing alumina matrix composite with single-wall carbon nanotubes. *Appl Phys Lett*. 2006;89:121910.
4. Wang Y, Wei F, Luo GH, Yu H, Gu GS. The large-scale production of carbon nanotubes in a nano-agglomerate fluidized-bed reactor. *Chem Phys Lett*. 2002;364(5–6):568–572.
5. Philippe R, Morancais A, Corrias M, Caussat B, Kihn Y, Kalck P, Plee D, Gaillard P, Bernard D, Serp P. Catalytic production of carbon nanotubes by fluidized-bed CVD. *Chem Vap Depos*. 2007;13: 447–457.
6. Philippe R, Serp P, Kalck P, Kihn Y, Bordère S, Plee D, Gaillard P, Bernard D, Caussat B. Kinetic study of carbon nanotubes synthesis by fluidized bed chemical vapor deposition. *AIChE J*. 2009;55:450–464.
7. Morancais A, Caussat B, Kihn Y, Kalck P, Plee D, Gaillard P, Bernard D, Serp P. A parametric study of the large scale production of multi-walled carbon nanotubes by fluidized bed catalytic chemical vapor deposition. *Carbon*. 2007;45:624–635.
8. Pirard SL, Pirard JP, Boussuot C. Modeling of a continuous rotary reactor for carbon nanotube synthesis by catalytic chemical vapor deposition. *AIChE J*. 2009;55:675–686.
9. Pirard SL, Heyen G, Pirard JP. Quantitative study of catalytic activity and catalytic deactivation of Fe-Co/Al_2O_3 catalysts for multi-walled carbon nanotube synthesis by CCVD process. *Appl Catal A Gen*. 2010;382:1–9.
10. Douven S, Pirard SL, Heyen G, Toye D, Pirard JP. Kinetic study of double-walled carbon nanotube synthesis by catalytic chemical vapour deposition over an Fe-Mo/MgO catalyst using methane as carbon. *Chem Eng J*. 2011;175:396–407.
11. Douven S, Pirard SL, Chan FY, Pirard R, Heyen G, Pirard JP. Large-scale synthesis of multi-walled carbon nanotubes in a continuous inclined mobile-bed rotating reactor by the catalytic chemical vapour deposition process using methane as carbon source. *Chem Eng J*. 2012;188:113–125.
12. Lee YT, Park J, Choi YS, Ryu H, Lee HJ. Temperature-dependent growth of vertically aligned carbon nanotube in the range 800–1100°C. *J Phys Chem B*. 2002;106:7614–7618.
13. Helveg S, Lopez-Cartes C, Sehested J, Hansen PL, Clausen BS, Rostrup-Nielsen JR, Albid-Pedersen F, Norskov JK. Atomic scale imaging of carbon nano fiber growth. *Nature*. 2004;427(6973):426–429.
14. Wirth CT, Zhang C, Zhong G, Hofmann S, Robertson J. Diffusion and reaction-limited growth of carbon nanotube forests. *ACS Nano*. 2009;3:3560–3566.
15. Anisimov AS, Nasibulin AG, Jiang H, Launois P, Cambedouzou J, Shandakov SD, Kauppinen EI. Mechanistic investigations of single-walled carbon nanotube synthesis by ferrocene vapor decomposition in carbon monoxide. *Carbon*. 2010;48:380–388.
16. Danafar F, Fakhrúl-Razi A, Salleh MAM, Baik DRA. Influence of catalytic particle size on the performance of fluidized-bed chemical vapor deposition synthesis of carbon nanotubes. *Chem Eng Res Des*. 2011;89:214–223.
17. Pirard SL, Douven S, Pirard JP. Analysis of kinetic models of multi-walled CNT synthesis. *Carbon*. 2007;45:3050–3052.
18. Liu K, Feng C, Chen Z, Fan S. A growth mark for studying growth mechanism of carbon nanotube arrays. *Carbon*. 2005;43: 2850–2856.
19. Dasgupta K, Joshi JB, Banerjee S. Fluidized bed synthesis of carbon nanotubes—a review. *Chem Eng J*. 2011;171:841–869.
20. Pirard S, Delafosse A, Toye D, Pirard J. Modeling of a continuous rotary reactor for carbon nanotube synthesis by catalytic chemical vapor deposition: influence of heat exchanges and temperature profile. *Chem Eng J*. 2013;232:488–494.
21. Corrias M, Caussat B, Ayral A, Durand J, Kihn Y, Kalck P, Serp P. Carbon nanotubes produced by fluidized bed catalytic CVD: first approach of the process. *Chem Eng Sci*. 2003;58(19):4475–4482.
22. Lamouroux E, Serp P, Klack P. Catalytic routes towards single wall carbon nanotubes. *Catal Rev*. 2007;49:341–405.
23. Venegoni D, Serp P, Feurer R, Kihn Y, Vahlas C, Kalck P. Parametric study for the growth of carbon nanotubes by catalytic chemical vapor deposition in a fluidized bed reactor. *Carbon*. 2002;40:1799–1807.
24. Philippe R, Caussat B, Falqui A, Kihn Y, Kalck P, Bordère S, Plee D, Gaillard P, Bernard D, Serp P. An original growth mode of MWCNTs on alumina supported iron catalysts. *J Catal*. 2009;263: 345–358.
25. Qian W, Wei F, Wang Z, Liu T, Yu H, Luo G, Lan X, Xiangyi D. Production of carbon nanotubes in a packed bed and a fluidized bed. *AIChE J*. 2003;49(3):619–625.
26. Yu H, Zhang Q, Wei F, Qian W, Luo G. Agglomerated CNTs synthesized in a fluidized bed reactor: agglomerate structure and formation mechanism. *Carbon*. 2003;41(14):2855–2863.
27. Qian W, Liu T, Wei F, Wang Z, Li Y. Enhanced production of carbon nanotubes: combination of catalyst reduction and methane decomposition. *Appl Catal A*. 2004;258:121–124.
28. Fakhru'l-Razi A, Danafar F, Radiah ABD, Mohd Salleh MA. An innovative procedure for large scale synthesis of carbon nanotubes by fluidized bed catalytic vapou deposition technique. Fullerenes. *Nanotubes Carbon Nanostruct*. 2009;17:652–663.
29. See CH, Dunens OM, MacKenzie KJ, Harris AT. Process parameter interaction effects during carbon nanotube synthesis in fluidized beds. *Ind Eng Chem Res*. 2008;47:7686–7692.
30. Harris AT, See CH, Liu J, Dunens O, MacKenzie KJ. Towards the large-scale synthesis of carbon nanotubes in fluidised beds. *J Nanosci Nanotechnol*. 2008;8:2450–2457.
31. Dasgupta K, Sen D, Mazumdar T, Lenka RK, Tewari R, Mazumder S, Joshi JB, Banerjee S. Formation of bamboo-shaped carbon nanotubes on carbon black in a fluidized bed. *J Nanopart Res*. 2012;14: 728–736.
32. Kunii D, Levenspiel O. *Fluidization Engineering*, 2nd ed. Newton: Butterworth-Heinemann, 1991.
33. Snoeck JW, Froment GF, Fowles M. Filamentous carbon formation and gasification: thermodynamics, driving force, nucleation, and steady-state growth. *J Catal*. 1997;169:250–262.
34. Hsieh CT, Lin YT, Chen WY, Wei JL. Parameter setting on growth of carbon nanotubes over transition metal/alumina catalysts in a fluidized bed reactor. *Powder Technol*. 2009;192:16–22.
35. Pirard SL, Douven S, Bossuot C, Heyen G, Pirard JP. A kinetic study of multi-walled carbon nanotube synthesis by catalytic

chemical vapour deposition using a Fe-Co/Al_2O_3 catalyst. *Carbon*. 2007;45:1167–1175.
36. Philippe R, Serp P, Kalck P, Bordère S, Plee D, Gaillard P, Bernard D, Caussat B. Kinetic modeling study of carbon nanotubes synthesis by fluidized bed chemical vapor deposition. *AIChE J*. 2009;55:465–474.
37. Gommes C, Blacher S, Bossuot C, Marchot P, Nagy JB, Pirard JP. Influence of the operating conditions on the production rate of multi-walled carbon nanotubes in a CVD reactor. *Carbon*. 2004;42:1473–1482.
38. Joshi JB, Ranade VV. Computational fluid dynamics for designing process equipment: expectations, current status and path forward. *Ind Eng Chem Res*. 2003;42:1115–1128.
39. Joshi JB, Sharma MM, Shah YT, Singh CPP, Ally M, Klinzing GE. Heat transfer in multiphase contactors. *Chem Eng Commun*. 1980;6:257–27.
40. Nere NK, Pathwardhan AW, Joshi JB. Liquid phase mixing in stirred vessels: turbulent flow regime. *Ind Eng Chem Res*. 2003;42:2661–2698.
41. Kumaresan T, Joshi JB. Effect of impeller design on flow pattern and mixing in stirred tanks. *Chem Eng J*. 2006;115:173–193.
42. Kulkarni AA, Joshi JB, Ravikumar V, Kulkarni BD. Application of multi-resolution analysis for simultaneous measurement of gas and liquid velocities and fractional gas hold up in bubble column using LDA. *Chem Eng Sci*. 2001;56:5037–5048.
43. Joshi JB, Tabib MV, Deshpande SS, Mathpati CS. Dynamics of flow structures and transport phenomena-1: experimental and numerical techniques for identification and energy content of flow structures. *Ind Eng Chem Res*. 2009;48:8244–8284.

Manuscript received Jan. 30, 2013, and revision received Mar. 15, 2014.